Detailed Study on the Failure of the Wedge Calibration Method at Nanonewton Setpoints for Friction Force Microscopy

Ortuso, Roberto Diego; Sugihara, Kaori

How to cite

ORTUSO, Roberto Diego, SUGIHARA, Kaori. Detailed Study on the Failure of the Wedge Calibration Method at Nanonewton Setpoints for Friction Force Microscopy. In: Journal of Physical Chemistry. C, 2018, vol. 122, n° 21, p. 11464–11474. doi: 10.1021/acs.jpcc.8b03583

This publication URL: https://archive-ouverte.unige.ch/unige:123228
Publication DOI: 10.1021/acs.jpcc.8b03583

The wedge calibration method at nanonewton forces for friction force microscopy

*Roberto D.Ortuso, Kaori Sugihara**

Department of Physical Chemistry, University of Geneva, Quai Ernest Ansermet 30,

1211 Geneva, Switzerland

* Corresponding Author: kaori.sugihara@unige.ch

Keywords

Friction force microscopy, wedge calibration method, nanotribology, lateral calibration coefficient

Abstract

The wedge calibration method is the most popular calibration technique in friction force microcopy for converting raw lateral laser deflection signals (in volt) into forces (in newton). Recent trends in nanotribology demand the use of the method at nanonewton (nN) force ranges, however, we found that this method fails at these small forces. The objective of the present work is to identify the reason why the conventional wedge calibration method fails at nN force ranges. We found that the equation used in the model in this method amplifies experimental errors by orders of magnitude only at small setpoints purely due to its mathematical expression. In general, signal-to-noise ratio is poor at small setpoints, thus this low tolerance against experimental errors in nanonewton force ranges completely gives an inconsistent calibration. We identified that the condition, under which the method operates accurately, is adhesion << setpoint. Discovery of this operation range (adhesion << setpoint) is important, because performing the calibration under other conditions can wrongly calibrate the system by orders of magnitude. Our result imposes a warning to the field that the conventional wedge calibration method has to be conducted at setpoints much larger than adhesion forces for the accurate calibration.

1. Introduction

Lateral force microscopy (LFM) is an atomic force microscopy (AFM)-based technique used in studies of frictions in tribology. The fact that AFM can control very small forces at nanonewton (nN) scale opened the field of nanotribology[1]. This significantly contributed to our understanding in the influence of lubrication in different matterials[2], which is important for selecting the right lubricants for extending the lifetime of machines[3]. Since the development of the LFM technique, the importance of friction studies is being recognized also in many other fields, including orientation guiding in crystals growth[4], fundamental studies in atomic interactions[5], and in the field of biomaterials science for characterizing the interaction between implants and surrounding body tissues[6].

In AFM, the deflection of the laser reflected on the backside of the cantilever is detected by a position sensitive detector (PSD). This raw signal includes two directions, “vertical deflection” that corresponds to the detection of vertical forces and “lateral deflection” for the cantilever torsion, hence the lateral forces. Both deflection signals have a unit of volt (V) due to the detection mechanism of the PSD. To correlate this deflection (in volt) into force (in newton) or distance (in meter), depending on the parameter of interest, users perform calibration procedures.

The calibration of the vertical deflection is straightforward, commonly performed by established methods known as thermal calibration method[7] or force-curve calibration method[8]. However, the calibration of lateral deflection is much more difficult mainly due to the fact that the measurement of torsional bending constant of cantilevers is more cumbersome. Two major classes of calibration methods have been developed for the lateral deflection[9].

The first class, known as indirect or multi-step techniques, requires an initial step that relates the applied lateral forces to the torsion of the cantilever, followed by a second procedure that correlates the torsion to the laser read out at the PSD[9]. These multi-step techniques include the method based on the direct force application on the cantilever by another AFM or optical tweezers[10], the static loading technique[11], the approach using lateral deflection of a reference beam[12], direct read out of a lateral force on a sensor plate[13] or a thermographic noise method of the torsional resonance frequency[14] combined with the torsional Sader method[15]. Geometrical cantilever analysis techniques[16,17], where the torsion spring constant is directly estimated from a high-resolution scanning electron microscopy (SEM) image of a cantilever and the properties of the material, are the other indirect techniques often used to calibrate the cantilever lateral deflection. Nevertheless, all the multi-step calibration techniques are labor-intensive, which makes their frequent use difficult during the AFM measurements. Thus, cantilevers are typically calibrated only once for a certain model of a cantilever, and the same calibration is used for the rest of all the experiments. It could potentially induce errors, because the tip from the same model from

the same manufacturer can have different properties due to the nanofabrication errors[18,19,20], and even an identical tip can alter its behavior over time due to the tip wearing[21].

The second class of torsional calibration techniques is known as direct or single-step techniques. The major advantage of these techniques is their simplicity to perform the single-step calibration directly by AFM without combining other tools such as SEM and optical tweezers. It enables the use of the calibration for multiple times during LFM experiments to assure the accuracy of the calibration. Among a number of approaches that fall into this class, the most accepted one is known as wedge calibration technique[9]. The technique was first developed by Ogletree et al. They succeeded in correlating the raw lateral signals (lateral deflection) to the lateral forces through a mathematical model that describes the force interactions between the integrated cantilever and a slope[22]. A single strontium titanate crystal, which naturally has an atomically defined grating (slopes), as a substrate and triangular integrated (pyramidal-shaped) tips were used in their work. Their mathematical model for processing the acquired scan-line data is the basis of the wedge calibration method. Other researchers[23], including Khare et al., have expanded this technique for the application towards spherical tip probes. Varenberg et al. further modified these method[24] for making it more intuitive and user-friendly. An important difference is that their model requires the measurement of a new parameter, adhesion F_{A}, which is separately quantified via force curves. Their approach has an advantage for eliminating some instrumental errors due to thermal drifts, which demanded an extra labor-intensive step in the original calibration method[22]. Their technique is also applicable both to integrated probes and colloidal-tip probes. A commercially available calibration grating was employed, which avoids the necessity of growing the crystal[25] used by Ogletree et al. A drawback of the wedge calibration method is that it heavily relies on the accuracy of the mathematical model. When the used models for the mechanical and physical description of the system are not appropriate, the technique is more prone to failure. Nevertheless, their wedge calibration method is among the most popular calibration technique in friction force microscopy, commonly used at the force range of micronewton to millinewton. However, its use at nanonewton force range has never been reported. In fact, we found that the method fails below several nanonewton setpoint.

The objective of the present work is to identify the reason why the conventional wedge calibration method fails in nanonewton force ranges. We found that the expression of the formula used in this model amplifies the experimental errors in the final output by orders of magnitude only at nanonewton setpoints. This extremely low tolerance against errors at small setpoints is the reason for the failure in this model, because experimentally errors are never zero in AFM at a finite signal to noise ratio.

2. Materials and methods

2.1. Atomic force microscopy

Atomic force microscopy (AFM) was carried out with NanoWizard® 3 AFM (JPK instruments, Berlin, Germany) equipped with AFM controller Software version 6.0.32. All the measurements were performed in an acoustic enclosure (JPK instruments, Berlin, Germany). Atmosphere within the enclosure was kept at fixed temperature ($T \approx 25$ °C) and at relative humidity under 10 %, where the effect of adsorbed water is negligible[26,27], by a continuous flow of filtered and humidity-reduced compressed air. Imaging was carried out in contact mode at the acquisition speed of 1 μm/s. During imaging, integral gain was kept at 110.0 ± 10 Hz, with a proportional gain of 0.002 ± 0.001. For each vertical stiffness, experiments were repeated with a few different AFM cantilevers for testing the reproducibility. For each tip, three areas were scanned per setpoint, yielding 606 images in total; (2 - 3 tips per one vertical cantilever stiffness) x (3 - 9 area) x (13 – 36 setpoints per tip). The area size was 10.0 μm (fast scanning direction) x (2.0 ± 0.1) μm with a pixel number of 128 x 25 ± 5. In total, the amount of the analyzed data was over 16'000 line scans.

2.2. Tips and calibration gratings

Table 1: Tip specifics, declared and measured.

			HQ:CSC38 - C (K_N = 0.03 N/m)	HQ:CSC38 - A (K_N = 0.09 N/m)	HQ:CSC37 - C (K_N = 0.3 N/m)
Declared	Tip Radius[28]	(nm)	< 30	< 30	< 35
	Length[29]	(μm)	350 ± 5	250 ± 5	350 ± 5
	Width[29]	(μm)	32.5 ± 3.0	32.5 ± 3.0	35.0 ± 3.0
	Thickness[30]	(μm)	1.5 ± 0.5	1.0 ± 0.5	2.0 ± 0.5
Measured	Vertical Stiffness K_N	(N/m)	0.028 ± 0.002	0.10 ± 0.02	0.32 ± 0.03
	Vertical Sensitivity S_N	(nm/V)	96 ± 38	59 ± 5	49 ± 1

All AFM tips used in this work were bought from Micromesh (Sofia, Bulgaria). Two specific series were used, each of which has three cantilevers with different stiffness. For higher stiffness cantilevers, the series HQ:CSC37 / Cr-Au was used. For medium and low stiffness cantilevers, the series HQ:CSC38

/ Cr-Au was used. As the cantilever vertical stiffness is a key aspect to estimate load and adhesion, each cantilever was calibrated through thermal noise calibration technique[7] available to the user within the AFM controller software. The parameters are listed in Table 1**.**

Prior to use all cantilevers were cleaned by plasma treatment (IoN 3MHz, PVATePla, California, USA) in argon atmosphere (PanGas, Dagmerstellen, Switzerland, Purity Grade: 5.0) for 25 minutes at 150 W power and 0.46 mbar pressure, as it was shown that tips are often heavily contaminated by packing and production residue[31]. The variation of the tip radius and the surface roughness due to this cleaning process is expected to be negligible[32]. These tips were then left in vacuum (< 20 mbar) at least overnight to reverse any surface activation[33]. TGF11 series, trapezoidal calibration grating with the average measured slope angle of 54.09° ± 0.14° (MicroMash, Sofia, Bulgaria), was cleaned by sonication in acetone (HPLC grade, Fisher Chemical, Pittsburg, USA), isopropanol (HPLC grade, Fisher Chemical, Pittsburg, USA), MilliQ water (EMD Millipore, Billerica, USA) twice to get rid of any chemical residues, dried with nitrogen (PanGas, Dagmerstellen, Switzerland, Purity Grade: 4.5), and stored under vacuum. After the tip was mounted on AFM and the grating was placed on the holder, the entire AFM setup was left in the enclosure for an additional one night to stabilize the temperature ($T \approx 25$ °C) and the relative humidity (< 10 %). During the experiments, the enclosure was opened for a short while only when the position of the grating was moved for scanning different areas. After these procedures, the enclosure was closed and we waited at least 20 min to re-stabilize the temperature and the humidity.

2.3. Adhesive force and line scan data analysis

Adhesion between the tip and the substrate (F_A) was extracted from force curves (Figure 1). The tip was approached from height of z = 2 μm towards the surface at an approach speed of 0.5 μm/s and was retracted at the same speed. At least nine force curves were taken per tip, per setpoint, per area, and their average values were used in the analysis. All force curves were handled with JPK-DP proprietary software version 6.0.36 (JPK instruments, Berlin, Germany). The baseline was removed (with an implemented software-function) and the lowest point in the retraction curve was taken to determine the adhesive force or pull-off force. AFM images were analyzed by a home-made program written with MATLAB® Software (MathWorks, Natick, USA) for processing the large amount of data. The actual setpoint that is read from the vertical deflection is often slightly different from the one that users specified. Therefore, the value directly measured by the instrument was used in the analysis to minimize the error[34]. Note that MATLAB® software digit precision is 32-bit, which is enough to process the raw data stored by the JPK measurement software (21-bit) accurately. Random data sets were manually analyzed to verify the consistency and correct functioning of the program.

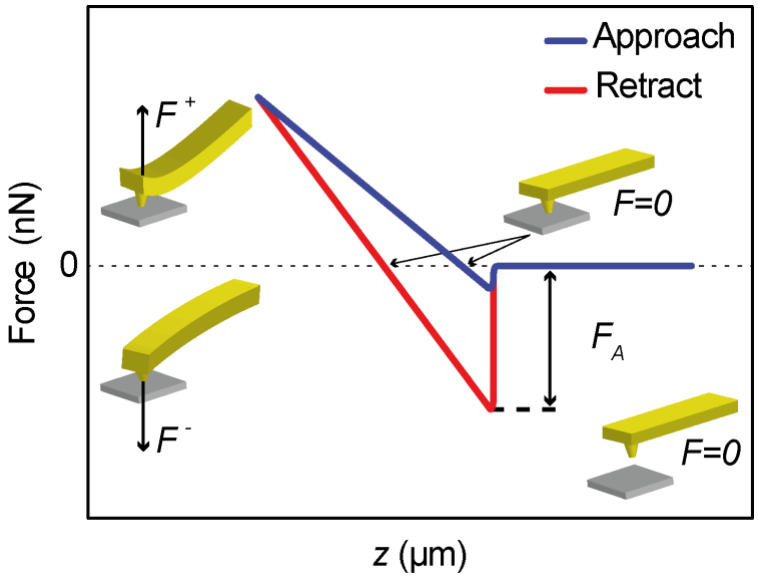

Figure 1: A scheme, showing ideal force curves for approach (blue) and retract (red), from which adhesion (F_A) is extracted.

2.4. Data fitting

Linear fitting was performed with the 'Curve Fitting Tool' in MATLAB®. A first order polynomial fitting was used according to the function:

$$y = f(x) = ax + b, \qquad \text{Eq. 1}$$

where a is the fixed and b, the *y*-intercept, is the open parameter. No robust fitting (e.g. least absolute residuals (LAR) or bi-square weights) was used as it would have weighted the data differently[35,36].

3. The wedge calibration theory[22, 24]

In this section, we outline the wedge calibration method developed by Ogletree et al.[22] and modified by Varenberg et al.[24] The equations only directly relevant to our work are shown, thus supplementary information and the original publications[22, 24] should be referred to for the details. The goal of the wedge calibration method is to obtain the calibration factor α, with which we can convert the raw lateral deflection signal W in the unit of volt (V) into lateral forces $F_{\parallel}$ in the unit of newton (N). Once the calibration factor α was obtained for a certain tip, LFM is ready to use with different substrates and even at different humidity.

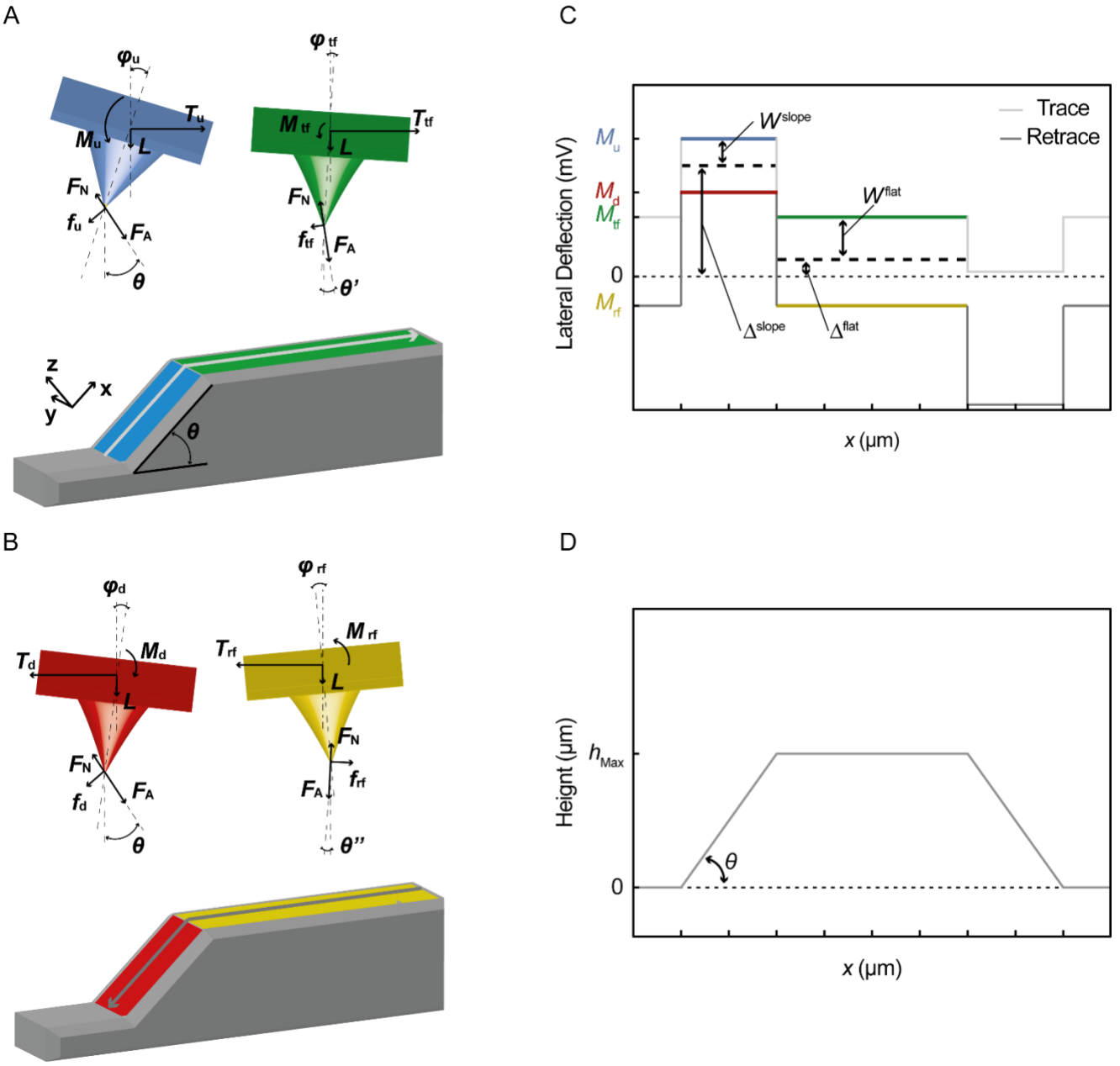

Figure 2: Schemes of the tip movement on a sloped surface (grating) (A) during uphill cantilever movement (from left to right) and (B) downhill cantilever movement (from right to left). (C) Ideal lateral deflection signals and (D) height profile, while scanning a sloped surface. Color code corresponds to the schemes.

The first step of the wedge calibration method is to obtain line scans of lateral deflection, while an AFM tip is scanning on a calibration grating with a known slope angle θ (Figure 2). These line scans enable the extraction of the sloped loop offset (Δ^{slope}), flat loop offset (Δ^{flat}), and the sloped half-width loop (W^{slope}) as indicated in Figure 2C. The second step is to measure the adhesion force between the tip and the substrate (F_{A}) from the force curves as described in section 2.3. The third step is to substitute

all the experimentally-measured parameters, L (load), F_A, Δ^{slope}, Δ^{flat}, W^{slope} and θ, into Eq. 2, which is a second order polynomial for the sloped friction coefficient (μ).

$$\sin\theta\,(L\cos\theta + F_{\mathrm{A}})\mu^2 - \frac{\Delta^{\mathrm{slope}} - \Delta^{\mathrm{flat}}}{W^{\mathrm{slope}}}(L + F_{\mathrm{A}}\cos\theta)\mu + L\cos\theta\sin\theta = 0\,. \qquad \text{Eq. 2}$$

Eq. 2 comes from the force and momentum balancing equations around the AFM tip, where the momentums are linked to the measured lateral deflection values (Δ^{slope}, Δ^{flat}, W^{slope}). Solving Eq. 2 yields two possible μ, because Eq. 2 is a second order polynomial. Through an evaluation procedure (see supplementary information or the original publications[24,22]) the correct μ will be selected. Finally, we substitute μ into Eq. 3 for obtaining the calibration factor α.

$$\frac{\mu(L + F_{\mathrm{A}}\cos\theta)}{\cos^2\theta - \mu^2\sin^2\theta} = \alpha W^{\mathrm{slope}}\,. \qquad \text{Eq. 3}$$

Note that μ mentioned above is a friction coefficient on the slope of the calibration grating. The friction coefficient at the flat part of the substrate can be estimated through the following Eq. 4.

$$\mu^{\mathrm{flat}} = \frac{\alpha W^{\mathrm{flat}}}{L + F_{\mathrm{A}}}\,. \qquad \text{Eq. 4}$$

In this method, both α and μ can be obtained from a single set of line scans (trace and retrace). This indicates that this method enables the calibration at a single setpoint, and also predicts the friction coefficient of substrates at a single setpoint, which is unusual, because friction coefficient is usually extracted from the slope of the $f = \mu F_{\mathrm{N}}$ curve, which requires measurements of lateral forces (f) at several setpoints (F_{N}).

4. Results and Discussion

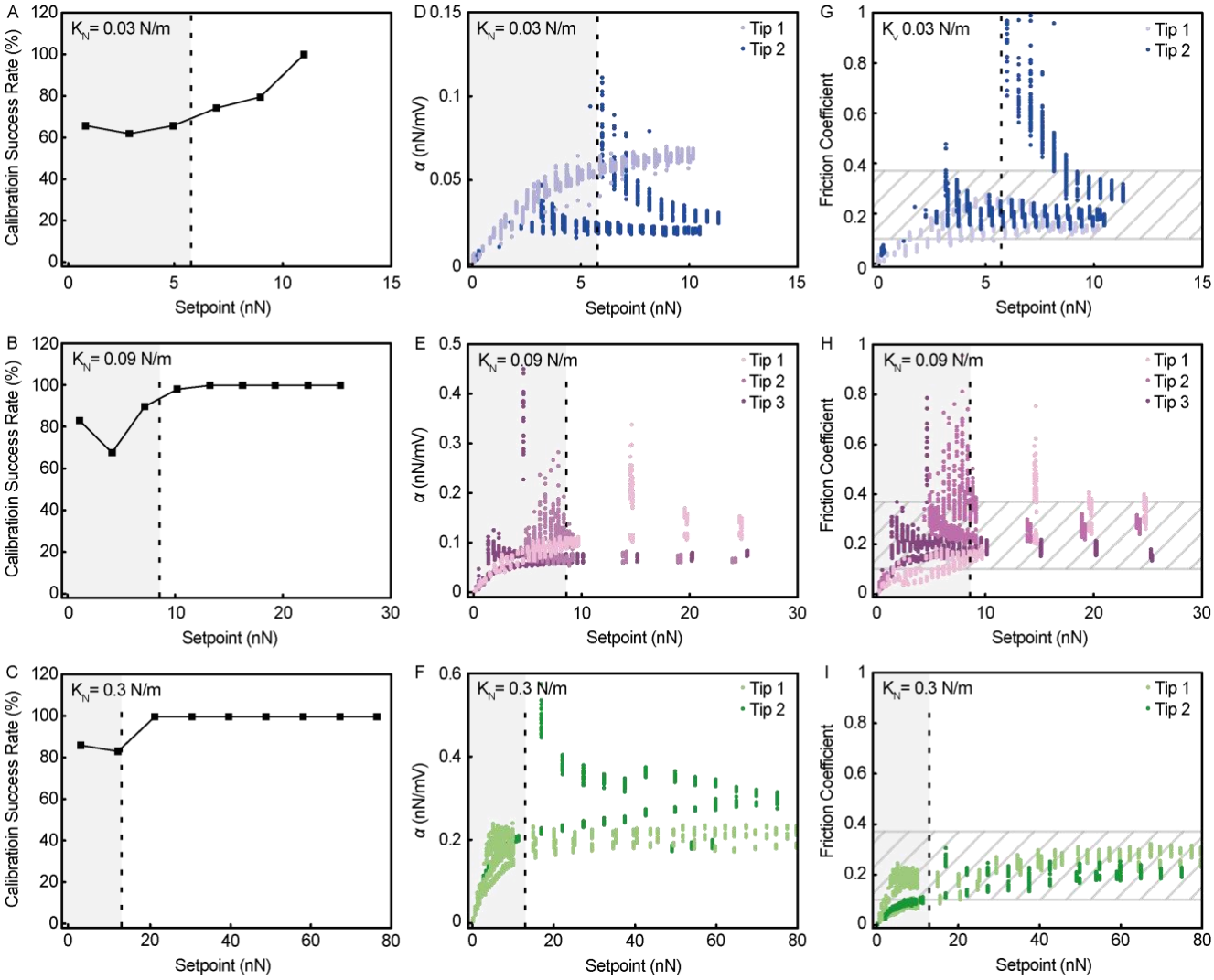

Figure 3: (A-C) Rate at which μ is in real domain vs setpoint. To simplify the figure, the value is averaged by a grouped setpoints. (A) Low stiffness tips (K_N = 0.03 N/m). Grouping interval: 0.5 nN. (B) Medium stiffness tips (K_N = 0.09 N/m). Grouping interval: 1.5 nN. (C) High stiffness tips (K_N = 0.3 N/m). Grouping interval: 4.5 nN. (D-F) Calibration coefficients (α) vs. setpoints. (D) Low stiffness tips (K_N = 0.03 N/m). (E) Medium stiffness tips (K_N = 0.09 N/m). (F) High stiffness tips (K_N = 0.3 N/m). (G-I) Friction coefficients vs. setpoints. (G) Low stiffness tips (K_N = 0.03 N/m). (H) Medium stiffness tips (K_N = 0.09 N/m). (I) High stiffness tips (K_N = 0.3 N/m). For all the plots, vertical dashed lines indicate the adhesion forces. Gray areas indicate the region, where setpoints are lower than adhesion forces (setpoint < adhesion). Horizontal areas with a diagonal grey pattern in (G-I) highlight friction coefficients' range reported in literature (0.1 – 0.37)[24,37,38,39-40].

Using the wedge calibration method proposed by Varenbergs et al. shown in section 3, first we present how the method fails at nanonewton force ranges. We selected three types of cantilevers with different bending modulus (K_N = 0.03 N/m – K_N = 0.3 N/m), and performed the wedge calibration method at effective setpoints ranging from 0.5 nN to 80 nN (note that the actual effective setpoint applied by AFM, extracted from the raw data and used for the calibration, is slightly different from user-input

setpoint). The starting point of the wedge calibration method is to substitute all the experimentally-determined parameters into Eq. 2 for obtaining μ. We noticed that the values of μ determined through Eq. 2 frequently fell into the imaginary domain at low setpoints (Figure 3A-C). This already implies that the method is not working at these setpoints, because an imaginary number as a friction coefficient makes no sense. Especially for the lowest stiffness tip (Figure 3A) this tendency is more prominent. Interestingly, the switching setpoint, below which μ tends to fall into imaginary domain, is close to the adhesion value (dotted vertical line in Figure 3A-C). This indicates that the wedge calibration method does not function properly when the setpoint is lower than the adhesion (gray zone in Figure 3A-C).

Next, for the cases, where μ was a real number, we substituted the obtained μ and the other necessary values into Eq. 3 for determining the calibration factor α. Obtaining α is the main goal of the wedge calibration method. With the calibration factor α we can convert the raw lateral deflection signal W in the unit of volt (V) into lateral forces $F_{\parallel}$ in the unit of newton (N) through an equation $F_{\parallel} = \alpha W$. Figure 3D-F presents the calculated α coefficients for cantilevers with different K_{N}. At high setpoints α saturates at constant values for all the tips. This is reasonable, because the calibration factor should be a constant value independent of the setpoints, as it represents the torsional bending modulus of the tip and the capabilities of AFM to read the signal[41,42,43]. Indeed, other techniques such as the geometrical calibration technique assume a constant value over the whole range of setpoints. However, when setpoints are smaller than adhesion (gray zones indicated in Figure 3D-F), α deviates from the saturation value, scatters, or goes to zero. This further indicates that the wedge calibration method is not working in this setpoint range.

In addition, Figure 3D-F highlights an interesting tip-dependency on α even if tips with exactly the same model from the same manufacturer were used. In multi-step calibration methods, typically the calibration is performed only once for a certain model of a tip and the calibration is used for the rest of the experiments. It is because the calibration procedure is so labor-intensive that it is difficult to integrate frequently between LFM experiments. Our results indicate the risk of approximating α for a certain model of tips.

The wedge calibration method further allows us to estimate friction coefficients between the used tips and the calibration grating μ^{flat} by substituting α into Eq. 4 with the half loop width (W^{flat}) of the flat trace (Figure 3G-I). Friction coefficients are only dependent on the two materials that are sliding between each other[44]. This value has often been used to confirm the accuracy of the calibration technique[45]. For our tip made of gold-plated silicon and the calibration grating made of silica, the flat friction coefficient should be in a range of (0.1 – 0.37)[24,37,38,39] (the range is indicated in Figure 3G-I), depending on the conditions of the surfaces[24,37,38,39]. Figure 3G-I shows that when the setpoints are much larger than

adhesions (adhesion << setpoint), the friction coefficient (μ^{flat}) saturates within these reported values for all the cantilevers with different K_{N}, while it deviates from the reported range when the setpoints are smaller than adhesive forces (setpoint < adhesion, grey areas in Figure 3G-I). It again suggests that the wedge calibration method is not functioning properly at setpoints below the adhesion value. The fact that we observed a similar trend for α and μ^{flat} (both failing below adhesion) is reasonable, because μ^{flat} is derived from α through Eq. 4. μ^{flat} values obtained as an average under the condition that the adhesive forces are much smaller than the setpoint (adhesion << setpoint, $\mu^{\mathrm{flat}}_{F_{\mathrm{A}}< L}$) are summarized in Table 2.

Table 2: Friction coefficients between the tips and the substrate obtained by averaging μ^{flat} (Figure 3G-I) in the range, where setpoints are higher than adhesion forces (adhesion < setpoint). All the μ^{flat} values are in agreement with the reported values in literature for gold – silica interface (0.1 – 0.37)[24,37,38,39].

	HQ:CSC38 - C (K_{N} = 0.03 N/m)		HQ:CSC38 - A (K_{N}= 0.09 N/m)			HQ:CSC37 - C (K_{N} = 0.3 N/m)	
	Tip 1	Tip 2	Tip 1	Tip 2	Tip 3	Tip 1	Tip 2
$\mu^{\mathrm{flat}}_{F_{\mathrm{A}}< L}$	0.15 ± 0.01	0.24 ± 0.06	0.27 ± 0.02	0.26 ± 0.09	0.18 ± 0.01	0.23 ± 0.06	0.20 ± 0.03

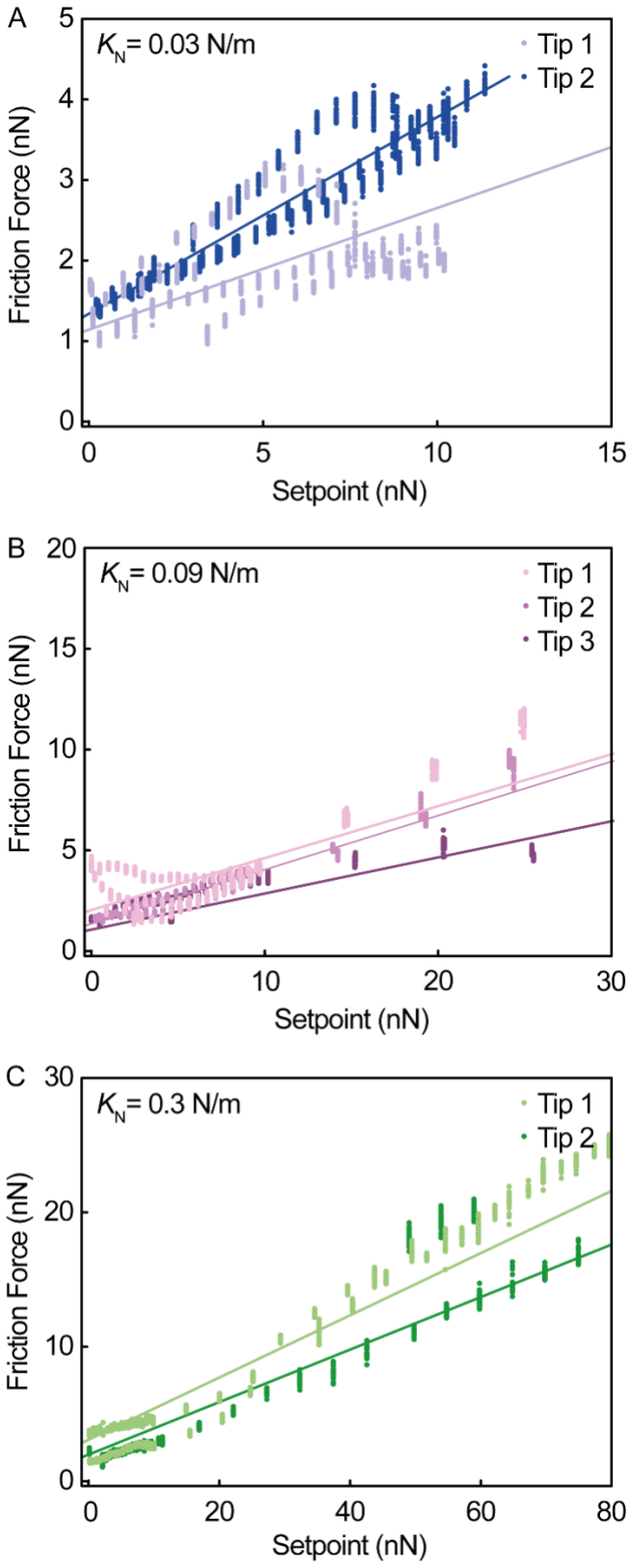

Figure 4: Friction forces vs. setpoints. (A) Low stiffness tips (K_N = 0.03 N/m). (B) Medium stiffness tips (K_N = 0.09 N/m). (C) High stiffness tips (K_N = 0.3 N/m). Lines indicate linear fitting with fixed friction coefficient.

Our results (Figure 3) strongly suggested that the both α and μ^{flat} can be accurately extracted only under the condition, where the adhesion is much smaller than the setpoint (adhesion << setpoint). Using these accurate calibration coefficients (α averaged over the range adhesion << setpoint, $\alpha_{F_{\mathrm{A}}<L}$), we converted raw lateral deflection W (V) at different setpoints into friction force (lateral force) (N) and plotted them against the setpoint in Figure 4. These plots should be accurate even at low setpoints below adhesion forces, because the values for α were estimated at setpoints well above adhesion force values. These plots in Figure 4 have non-zero *y*-intercepts, which are especially visible for low K_{N} tips (Figure 4AB). This corresponds to the friction law used the wedge calibration method $f = \mu^{\mathrm{flat}}(F_{\mathrm{N}} + F_{\mathrm{A}})$, where $f \neq 0$ when F_{N} = 0. These *y*-intercepts (b) can be estimated by fitting the data with $f = \mu^{\mathrm{flat}}_{F_{\mathrm{A}}<L} F_{\mathrm{N}} + b$, where $\mu^{\mathrm{flat}}_{F_{\mathrm{A}}<L}$ is the value shown in Table 2 (the results shown in Table 3). First, $\mu^{\mathrm{flat}}_{F_{\mathrm{A}}<L}$ fits the slope of the friction force vs setpoint curves reasonably (fitting curves shown in Figure 4), indicating that the friction coefficient that this method provides at a single setpoint matches with the one estimated from the slope of the friction force vs setpoint curve. Second, the extracted *y*-intercepts are in agreement with what the model assumes ($\mu^{\mathrm{flat}}_{F_{\mathrm{A}}<L} F_{\mathrm{A}}$), both of which illustrate the consistency of the model (Table 3).

Table 3: *y*-intercepts extracted from the linear fittings in Figure 4.

Fit Eq. $\mu^{\mathrm{flat}}_{F_{\mathrm{A}}<L} F_{\mathrm{N}} + b$	HQ:CSC38 - C (K_{N} = 0.03 N/m)		HQ:CSC38 - A (K_{N} = 0.09 N/m)			HQ:CSC37 - C (K_{N} = 0.3 N/m)	
	Tip 1	Tip 2	Tip 1	Tip 2	Tip 3	Tip 1	Tip 2
b	1.15	1.34	2.03	1.34	1.06	3.05	1.94
$\mu^{\mathrm{flat}}_{F_{\mathrm{A}}<L} F_A$	0.84	1.39	2.01	1.43	1.95	3.13	0.24

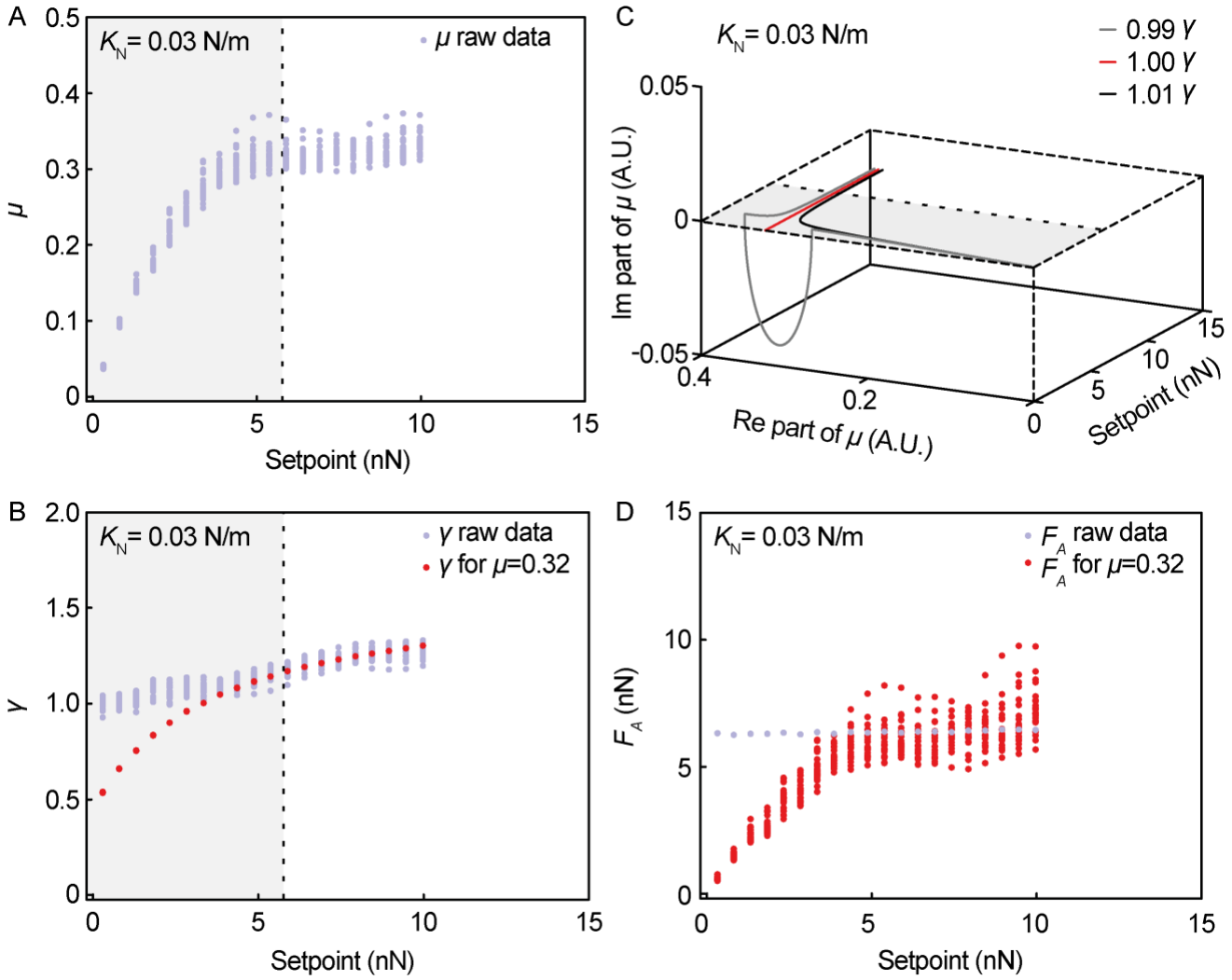

Figure 5: (A) μ calculated from the experimentally determined parameters vs. load. Gray area indicate the region where setpoints are lower than adhesion forces (setpoint < adhesion). (B) "Ideal Υ" ($\Upsilon = \frac{\Delta^{\text{slope}} - \Delta^{\text{flat}}}{W^{\text{slope}}}$), where μ = 0.322 (the "correct" high-force-end value) and the measured adhesion force (F_A) were used, vs setpoints (in red) together with experimentally-measured Υ (in light blue). Gray area indicate the region where setpoints are lower than adhesion forces (setpoint < adhesion). (C) μ for Υ with different errors (0%, $\pm$ 1%) vs. setpoint. Gray area on real plain indicates the region where setpoints are lower than adhesion forces (setpoint < adhesion). (D) Adhesion force vs. setpoint. The adhesion experimentally obtained (in blue) and the "ideal F_A" (F_A for μ = 0.322, in red) that would have yielded μ = 0.322 throughout the whole setpoint range.

Our next goal is to identify the origin of the failure at small setpoints. The model used in the method presents reasonable consistency as discussed above, thus is unlikely to be the reason for this problem. To study whether the failure is attributed to the errors in the experimentally-determined parameters (F_A, $\Delta^{\text{slope}} - \Delta^{\text{flat}}$, W^{slope}), we investigated the propagation of these errors into the final parameters such as μ through the equations. In following, we will explain the main finding with an example of a set of data from the lowest K_N tip (K_N = 0.03 N/m).

In the wedge calibration method, our first task is to solve the second order polynomial equation for μ (Eq. 2) by substituting experimentally obtained parameters. The result yields μ as a function of load (setpoint, L) as plotted in Figure 5A, which highlights how the method fails at small setpoints as mentioned previously. Now we assume that this failure originates from the errors in the experimentally determined parameters (F_{A}, $\Delta^{\mathrm{slope}} - \Delta^{\mathrm{flat}}$, W^{slope}) that were substituted into Eq. 2.

First, we supposed that the error is in $\Upsilon = \frac{\Delta^{\mathrm{slope}} - \Delta^{\mathrm{flat}}}{W^{\mathrm{slope}}}$, while the adhesion force (F_{A}) is correct. To evaluate this possible error in the parameter, we solved the Eq. 2 for Υ and substituted measured F_{A} and μ = 0.322 (the "correct" high-force-end value for μ). The goal of this analysis is to simulate an "ideal Υ" that would have produced a constant μ = 0.322 throughout the whole range of the used L . The result is plotted in Figure 5B in red together with the experimentally measured Υ (in light blue) against load (L). At large loads, the "ideal Υ" and the actual experimental results match very well, which explains why obtained μ was accurate in this force range. At the lower setpoints, however, they are noticeably different. In other words, this deviation of the experimental values from the ideal ones can be attributed to the reason for the error in μ at small setpoints.

Nevertheless, this deviation is not more than 86% at around 0 nN, while the final error in μ at these small setpoints is over 10,000%. It is surprising that such a moderate experimental error completely alters the orders of magnitude of μ (and thus α). Therefore, to understand the reason for this error amplification, next we evaluated how this error in Υ propagates into μ through the Eq. 2. Figure 5C illustrates the obtained μ in the cases, where Υ has $\pm$1% deviation compared to the "ideal Υ". First, the "ideal Υ" (1.00 Υ in red) yields μ = 0.322 throughout the whole range of the load, because this is how we defined it. Surprisingly, inducing $\pm$1% error in Υ completely alters μ by orders of magnitudes at low setpoints, where already in the case with $-$1% error (0.99 Υ) it even fell into the imaginary domain. These behaviors of μ, where μ either goes to imaginary domain, zero or scatters at setpoints below adhesion, well resembles what we observed in Figure 3. This suggests that Eq. 2 is extremely sensitive to the error in Υ at small setpoints. The threshold load (L_{Th}), under which μ starts to deviate from the high end value (μ = 0.322) more than 2%, was derived as $L_{\mathrm{Th}} = 0.73F_{\mathrm{A}}$ (see SI for the detail). This explains why the method systematically failed at around setpoints below adhesion ($L_{\mathrm{Th}} \approx F_{\mathrm{A}}$). Experimentally, a certain amount of error is unavoidable under a limited signal-to-noise ratio, which becomes much worse at lower setpoints due to the small signals. Therefore the model's extremely low tolerance against the error at setpoints below adhesion and the decreased signal-to-noise ratio in these setpoints are the main origin of the failure.

Next, we investigated whether the failure at small setpoints can be attributed to the experimental errors in adhesion, F_{A}. In this case, we assumed that the experimentally-obtained Υ is accurate. We

solve the Eq. 2 for F_A by substituting μ = 0.322 (saturation value at high force) and the experimentally-obtained Υ. Similarly to the previous case, the purpose of this analysis is to see how adhesion F_A should look like if we want to have the correct constant μ = 0.322 throughout the whole range of the measured loads. These calculated adhesion values are plotted in Figure 5D in red together with the adhesion we measured from the pull-off force in light blue. These results suggest that the adhesion, F_A, has to be nearly of 0 nN at L = 0 nN for obtaining the correct μ. However, this is not reasonable, because friction force vs load plot in Figure 4 implicates that the adhesion is non-zero (F_A = 6.32 nN) at L = 0 nN. This result suggests that the final error in μ and α cannot be explained just with the error in F_A.

To conclude, although we expect unavoidable experimental errors in all the measured values F_A, $\Delta^{\text{slope}} - \Delta^{\text{flat}}$, W^{slope}, the major contribution to the problem we faced at small setpoints is due to $\Upsilon = \frac{\Delta^{\text{slope}} - \Delta^{\text{flat}}}{W^{\text{slope}}}$, because in case of Υ the error is amplified by orders of magnitude into the final value of μ due to the shape of Eq. 2. The error in F_A probably also exists as the pull-off force is not an ideal estimator for the adhesive force in a sliding contact, which could be an additional factor for the error.

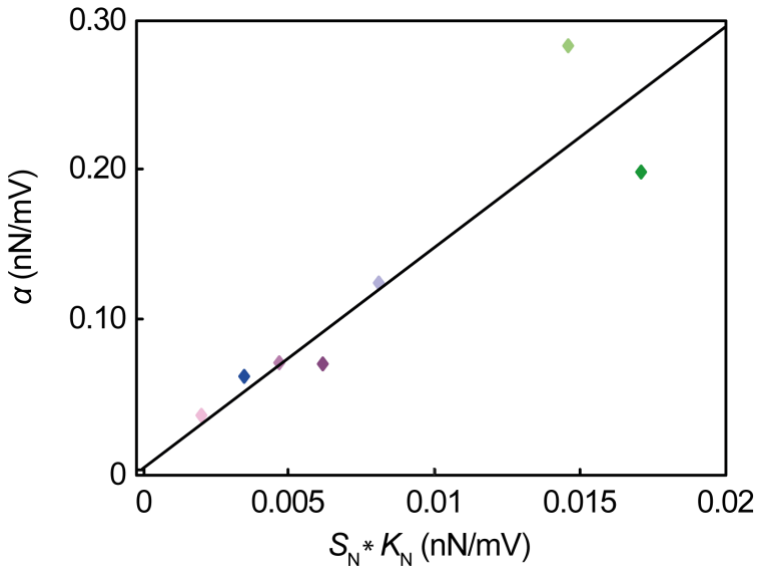

Figure 6: $\alpha_{F_A < L}$ vs. vertical calibration factors with linear fitting. Color code corresponds to the one used for the tips from Figure 3D-I.

Finally, these $\alpha_{F_A < L}$ (the correct alpha estimated well above the adhesion) are plotted against vertical calibration factors (VCF) in Figure 6, where the vertical calibration factors are the multiplication of the vertical sensitivity (S_N) and vertical stiffness (K_N), both of which represent the properties of tips in vertical direction and can be measured by the standard procedure integrated in the AFM software. The

linear relationship between α and VCF implies that the torsional bending modulus (α) and the vertical bending modulus are linked. The torsional bending modulus is defined by the mechanical properties of the material, technological and the geometrical characteristics of the tips. The same parameters also define the VCF. Therefore, theoretically these two coefficients (α and VCF) are linked through tip and instrumental parameters and should present a well-known relationship[46,47] expressed as

$$\alpha = \left(\frac{S_\theta}{S_N}\,\frac{4Gl^2}{3Eh^2}\right)(S_N * K_N). \qquad \text{Eq. 5}$$

Note that the S_N in the numerator and the denominator can be canceled out, yet we left as they are to explicitly show the parameter VCF ($S_N * K_N$). Indeed Figure 6 shows a linear relationship between α and VCF, where a linear fitting yields a slope coefficient of 14.74. This relationship is convenient, because it implies that α can be roughly estimated as $\alpha = 14.74\ (S_N * K_N)$ even without performing the lateral calibration, as long as the same type of tips (material, coating, shape) and AFM are used.

Conclusion

We identified that the model's low tolerance against errors combined with decreased signal-to-noise ratio at low setpoints are the reason why the original Varenberg method fails at nanoscale. We clarified that this failure occurs when setpoints are chosen either at the same orders of magnitude or below adhesion. Discovery of this operation range (adhesion << setpoint) is extremely important, because performing the calibration under other conditions can wrongly calibrate the system by orders of magnitude. As long as it is conducted at setpoints well above the adhesion, the exact procedure described by Varenberg yields accurate calibration. It is curious to see how the model fails only at small setpoints even if we assumed a constant error throughout the whole range of setpoints in our analysis. This is because the problem purely comes from the shape of Eq. 2, which amplifies the experimental errors in the final results only under a certain condition. Our result imposes a warning to the field that the conventional wedge calibration method has to be conducted at setpoints much larger than adhesion forces for extracting an accurate α.

Acknowledgements

Part of the research leading to these results has received funding from Swiss National Science Foundation (200021_162425).

Bibliography

1. Bhushan, B., Nanotribology and Nanomechanics. *Wear* **2005**, *259*, 1507-1531.
2. Kano, M.; Yasuda, Y.; Ye, J., The Effect of Zddp and Modtc Additives in Engine Oil on the Friction Properties of Dlc‐Coated and Steel Cam Followers. *Lubrication Science* **2004**, *17*, 95-103.
3. Eger, G.; Laughlin, R., Evolution of Drive Systems for Work Tool Machines. **1966**, *1*, 7148-7191.
4. Gnecco, E.; Bennewitz, R.; Gyalog, T.; Meyer, E., Friction Experiments on the Nanometre Scale. *Journal of Physics: Condensed Matter* **2001**, *13*, 619-642.
5. Socoliuc, A.; Bennewitz, R.; Gnecco, E.; Meyer, E., Transition from Stick-Slip to Continuous Sliding in Atomic Friction: Entering a New Regime of Ultralow Friction. *Physical review letters* **2004**, *92*, 134301.
6. Alonso, J. L.; Goldmann, W. H., Feeling the Forces: Atomic Force Microscopy in Cell Biology. *Life Sciences* **2003**, *72*, 2553-2560.
7. Hutter, J. L.; Bechhoefer, J., Calibration of Atomic‐Force Microscope Tips. *Review of Scientific Instruments* **1993**, *64*, 1868-1873.
8. Cappella, B.; Dietler, G., Force-Distance Curves by Atomic Force Microscopy. *Surface science reports* **1999**, *34*, 1-104.
9. Munz, M., Force Calibration in Lateral Force Microscopy: A Review of the Experimental Methods. *Journal of Physics D: Applied Physics* **2010**, *43*, 063001.
10. Reitsma, M. G., Lateral Force Microscope Calibration Using a Modified Atomic Force Microscope Cantilever. *Review of Scientific Instruments* **2007**, *78*, 106102.
11. Cain, R. G.; Biggs, S.; Page, N. W., Force Calibration in Lateral Force Microscopy. *Journal of Colloid and Interface Science* **2000**, *227*, 55-65.
12. Liu, W.; Bonin, K.; Guthold, M., Easy and Direct Method for Calibrating Atomic Force Microscopy Lateral Force Measurements. *Review of Scientific Instruments* **2007**, *78*, 063707.
13. Ando, Y.; Shiraishi, N., Development of a Microlateral Force Sensor and Its Evaluation Using Lateral Force Microscopy. *Review of Scientific Instruments* **2007**, *78*, 033701.
14. Yaxin, S.; Bharat, B., Atomic Force Microscopy Dynamic Modes: Modeling and Applications. *Journal of Physics: Condensed Matter* **2008**, *20*, 225012.
15. Green, C. P.; Lioe, H.; Cleveland, J. P.; Proksch, R.; Mulvaney, P.; Sader, J. E., Normal and Torsional Spring Constants of Atomic Force Microscope Cantilevers. *Review of Scientific Instruments* **2004**, *75*, 1988-1996.
16. Liu, E.; Blanpain, B.; Celis, J. P., Calibration Procedures for Frictional Measurements with a Lateral Force Microscope. *Wear* **1996**, *192*, 141-150.
17. Palacio, M. L.; Bhushan, B., Normal and Lateral Force Calibration Techniques for Afm Cantilevers. *Critical Reviews in Solid State and Materials Sciences* **2010**, *35*, 73-104.
18. Mendels, D.-A.; Lowe, M.; Cuenat, A.; Cain, M. G.; Vallejo, E.; Ellis, D.; Mendels, F., Dynamic Properties of Afm Cantilevers and the Calibration of Their Spring Constants. *Journal of Micromechanics and Microengineering* **2006**, *16*, 1720-1733.
19. Grow, R. J.; Minne, S. C.; Manalis, S. R.; Quate, C. F., Silicon Nitride Cantilevers with Oxidation-Sharpened Silicon Tips for Atomic Force Microscopy. *Journal of Microelectromechanical Systems* **2002**, *11*, 317-321.
20. Albrecht, T. R.; Akamine, S.; Carver, T.; Quate, C. F., Microfabrication of Cantilever Styli for the Atomic Force Microscope. *Journal of Vacuum Science & Technology A: Vacuum, Surfaces, and Films* **1990**, *8*, 3386-3396.
21. Chung, K.-H.; Lee, Y.-H.; Kim, D.-E., Characteristics of Fracture During the Approach Process and Wear Mechanism of a Silicon Afm Tip. *Ultramicroscopy* **2005**, *102*, 161-171.
22. Ogletree, D.; Carpick, R. W.; Salmeron, M., Calibration of Frictional Forces in Atomic Force Microscopy. *Review of Scientific Instruments* **1996**, *67*, 3298-3306.

23. Khare, H.; Burris, D., The Extended Wedge Method: Atomic Force Microscope Friction Calibration for Improved Tolerance to Instrument Misalignments, Tip Offset, and Blunt Probes. *Review of Scientific Instruments* **2013**, *84*, 055108.
24. Varenberg, M.; Etsion, I.; Halperin, G., An Improved Wedge Calibration Method for Lateral Force in Atomic Force Microscopy. *Review of Scientific Instruments* **2003**, *74*, 3362-3367.
25. Nassau, K.; Miller, A. E., Strontium Titanate: An Index to the Literature on Properties and the Growth of Single Crystals. *Journal of Crystal Growth* **1988**, *91*, 373-381.
26. Liu, H.; Bhushan, B., Nanotribological Characterization of Molecularly Thick Lubricant Films for Applications to Mems/Nems by Afm. *Ultramicroscopy* **2003**, *97*, 321-340.
27. Sedin, D. L.; Rowlen, K. L., Adhesion Forces Measured by Atomic Force Microscopy in Humid Air. *Analytical Chemistry* **2000**, *72*, 2183-2189.
28. Sedin, D. L.; Rowlen, K. L., Influence of Tip Size on Afm Roughness Measurements. *Applied Surface Science* **2001**, *182*, 40-48.
29. Dimitrov, D.; Van Wijck, W.; Schreve, K.; De Beer, N., Investigating the Achievable Accuracy of Three Dimensional Printing. *Rapid Prototyping Journal* **2006**, *12*, 42-52.
30. Chen, C. C.; Sullivan, P. A. In *Solving the Mystery-the Problem of Z-Height Inaccuracy of the Stereolithography Parts*, The Sixth International Conference on Rapid Prototyping, 1995.
31. Busuttil, K.; Nikogeorgos, N.; Zhang, Z.; Geoghegan, M.; Hunter, C. A.; Leggett, G. J., The Mechanics of Nanometre-Scale Molecular Contacts. *Faraday discussions* **2012**, *156*, 325-341.
32. Berman, D.; Krim, J., Impact of Oxygen and Argon Plasma Exposure on the Roughness of Gold Film Surfaces. *Thin Solid Films* **2012**, *520*, 6201-6206.
33. Tsai, H.; Hu, E.; Perng, K.; Chen, M.; Wu, J.-C.; Chang, Y.-S., Instability of Gold Oxide Au2o3. *Surface Science* **2003**, *537*, 447-450.
34. Hues, S. M.; Draper, C. F.; Lee, K. P.; Colton, R. J., Effect of Pzt and Pmn Actuator Hysteresis and Creep on Nanoindentation Measurements Using Force Microscopy. *Review of scientific instruments* **1994**, *65*, 1561-1565.
35. Berk, R., A Primer on Robust Regression. In *Modern Methods of Data Analysis.*, John Fox; Long, J. S., Eds. Sage Publications: London, 1990; pp 293 - 325.
36. Miller, J. N., Basic Statistical Methods for Analytical Chemistry. Part 2. Calibration and Regression Methods. A Review. *Analyst* **1991**, *116*, 3-14.
37. Tocha, E.; Schonherr, H.; Vancso, G. J., Quantitative Nanotribology by Afm: A Novel Universal Calibration Platform. *Langmuir* **2006**, *22*, 2340-2350.
38. Bhushan, B.; Li, X., Micromechanical and Tribological Characterization of Doped Single-Crystal Silicon and Polysilicon Films for Microelectromechanical Systems Devices. *Journal of Materials Research* **1997**, *12*, 54-63.
39. Gabriel, K.; Behi, F.; Mahadevan, R.; Mehregany, M., In Situ Friction and Wear Measurements in Integrated Polysilicon Mechanisms. *Sensors and Actuators A: Physical* **1990**, *21*, 184-188.
40. Vancso, G. J.; Förster, S.; Leist, H., Nanometer-Scale Tribological Properties of Highly Oriented Thin Films of Poly(Tetrafluoroethylene) Studied by Lateral Force Microscopy. *Macromolecules* **1996**, *29*, 2158-2162.
41. Feiler, A.; Attard, P.; Larson, I., Calibration of the Torsional Spring Constant and the Lateral Photodiode Response of Frictional Force Microscopes. *Review of scientific instruments* **2000**, *71*, 2746-2750.
42. Jaschke, M.; Butt, H. J., Height Calibration of Optical Lever Atomic Force Microscopes by Simple Laser Interferometry. *Review of scientific instruments* **1995**, *66*, 1258-1259.
43. Gates, R. S.; Pratt, J. R., Accurate and Precise Calibration of Afm Cantilever Spring Constants Using Laser Doppler Vibrometry. *Nanotechnology* **2012**, *23*, 375702.
44. Blau, P. J., The Significance and Use of the Friction Coefficient. *Tribology International* **2001**, *34*, 585-591.
45. Wang, H.; Gee, M. L., Afm Lateral Force Calibration for an Integrated Probe Using a Calibration Grating. *Ultramicroscopy* **2014**, *136*, 193-200.

46. Miller, S. A.; Macdonald, N. C.; Xu, Y. Microfabricated Torsional Cantilevers for Sensitive Force Detection. US 08/683,929, 1997.
47. Malekian, M.; Park, S.; Strathearn, D.; Mostofa, M. G.; Jun, M., Atomic Force Microscope Probe-Based Nanometric Scribing. *Journal of Micromechanics and Microengineering* **2010**, *20*, 115016.

For Table of Contents Only (TOC)